Supporting Information

Light-guided intrabodies for on-demand *in-situ* target recognition in human cells

Eike F. Joest[1], Christian Winter[1], Joshua S. Wesalo[2], Alexander Deiters[2], Robert Tampé[1,*]

[1] Institute of Biochemistry, Biocenter, Goethe University Frankfurt, Max-von-Laue-Str. 9, 60438 Frankfurt, Germany

[2] Department of Chemistry, University of Pittsburgh, 219 Parkman Avenue, Pittsburgh, Pennsylvania 15260, USA

Table of Contents for Supporting Information

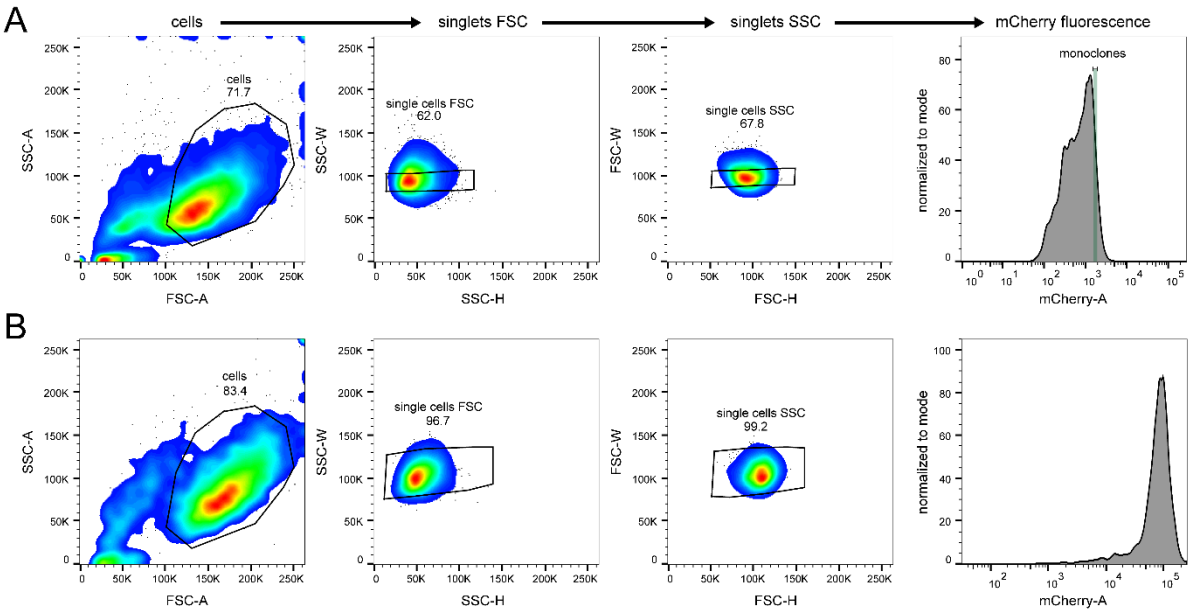

Supplementary Fig. 1 | Flow cytometry gating strategy. For generation of monoclonal cell lines and amber-construct expression analysis. 5000 events were recorded per sample. Shares of parent populations are provided for each gate. (A) representative FACS plots for selection of monoclonal cells. Single cells with high $^{Amb}Nb^{mcherry}$ expression were sorted into distinct wells after doublet discrimination. (B) representative FACS plots for amber-construct expression analysis. mCherry excitation laser intensities were different.

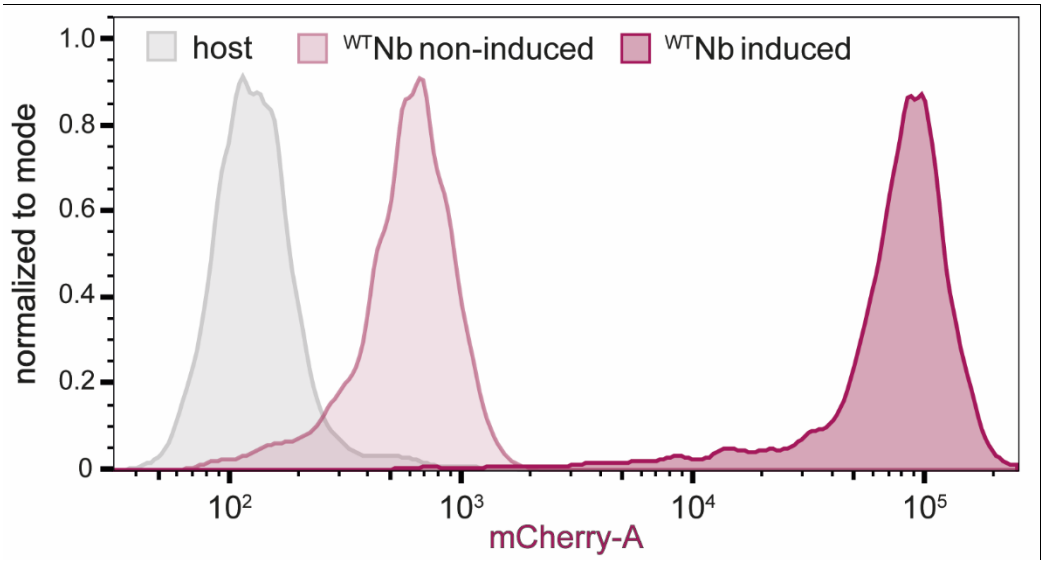

Supplementary Fig. 2 | Expression of wild-type intrabody in stable cells monitored by flow cytometry. Tetracycline-induced expression of $^{WT}Nb^{mCherry}$ evokes a strong mCherry fluorescence. Cell counts were normalized to mode (n = 3).

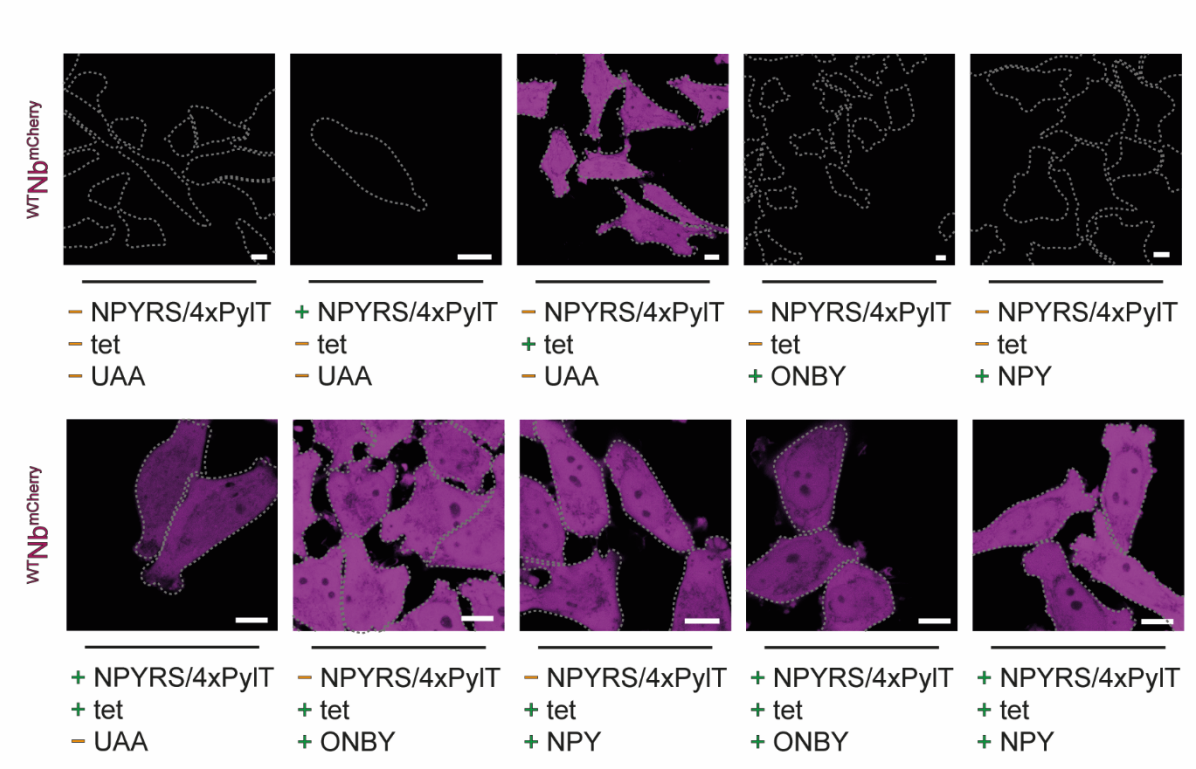

Supplementary Fig. 3 | Expression of wild-type intrabody $^{WT}Nb^{mCherry}$ in stable cells. Tetracycline-induced expression of intrabodies monitored by mCherry. Expression was not affected by the presence of amber suppression components. Live-cell CLSM imaging. Dashed lines indicate cellular borders. Scale bar, 10 µm.

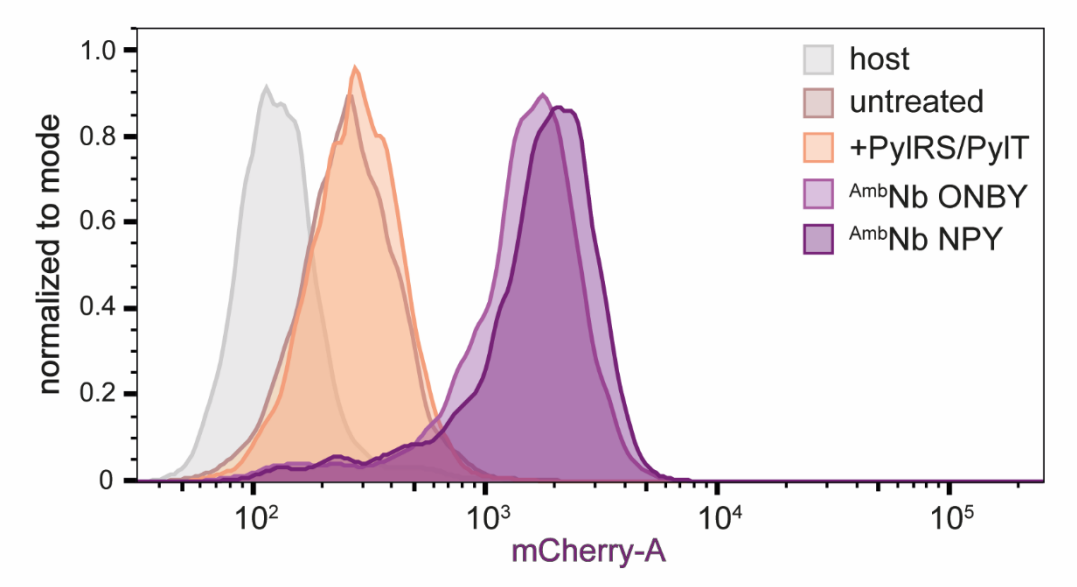

Supplementary Fig. 4 | Expression of amber-construct $^{Amb}Nb^{mCherry}$ monitored by flow cytometry. The early amber stop codon mutation Tyr37TAG abolished expression without optimized amber-suppression conditions. Suppression of the amber stop codon resulted in incorporation of photocaged amino acids and hence in intrabody expression. Expression was observed by downstream encoded mCherry. ^{Amb}Nb ONBY/NPY show amber suppression conditions with respective photocaged tyrosine. Counts of stable cells were normalized to mode (n = 3).

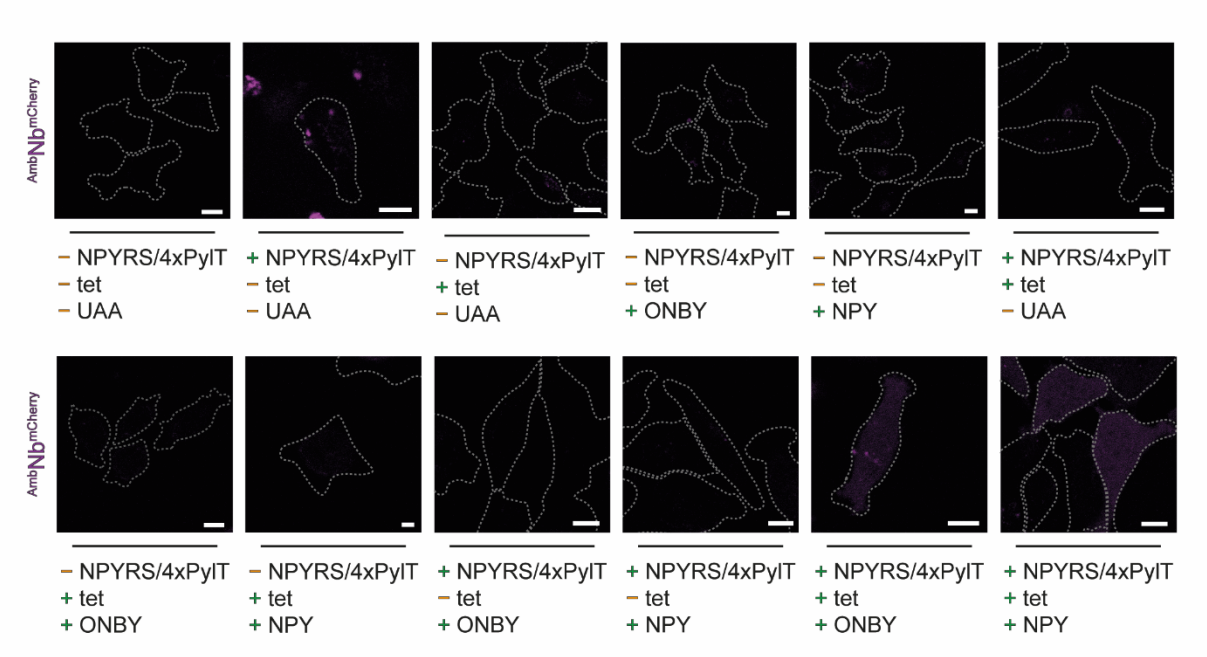

Supplementary Fig. 5 | Expression of amber-construct $^{Amb}Nb^{mCherry}$ by CLSM. The early amber stop codon (Tyr37TAG) abolished expression in the absence of the tRNA/NYPRS pair and/or the unnatural amino acid (UAA). Suppression of the amber stop codon resulted in incorporation of photocaged amino acids and hence in intrabody expression. Expression was observed by downstream encoded mCherry. Live-cell imaging of stable cell line. Dashed lines indicate cell borders. Scale bar, 10 µm.

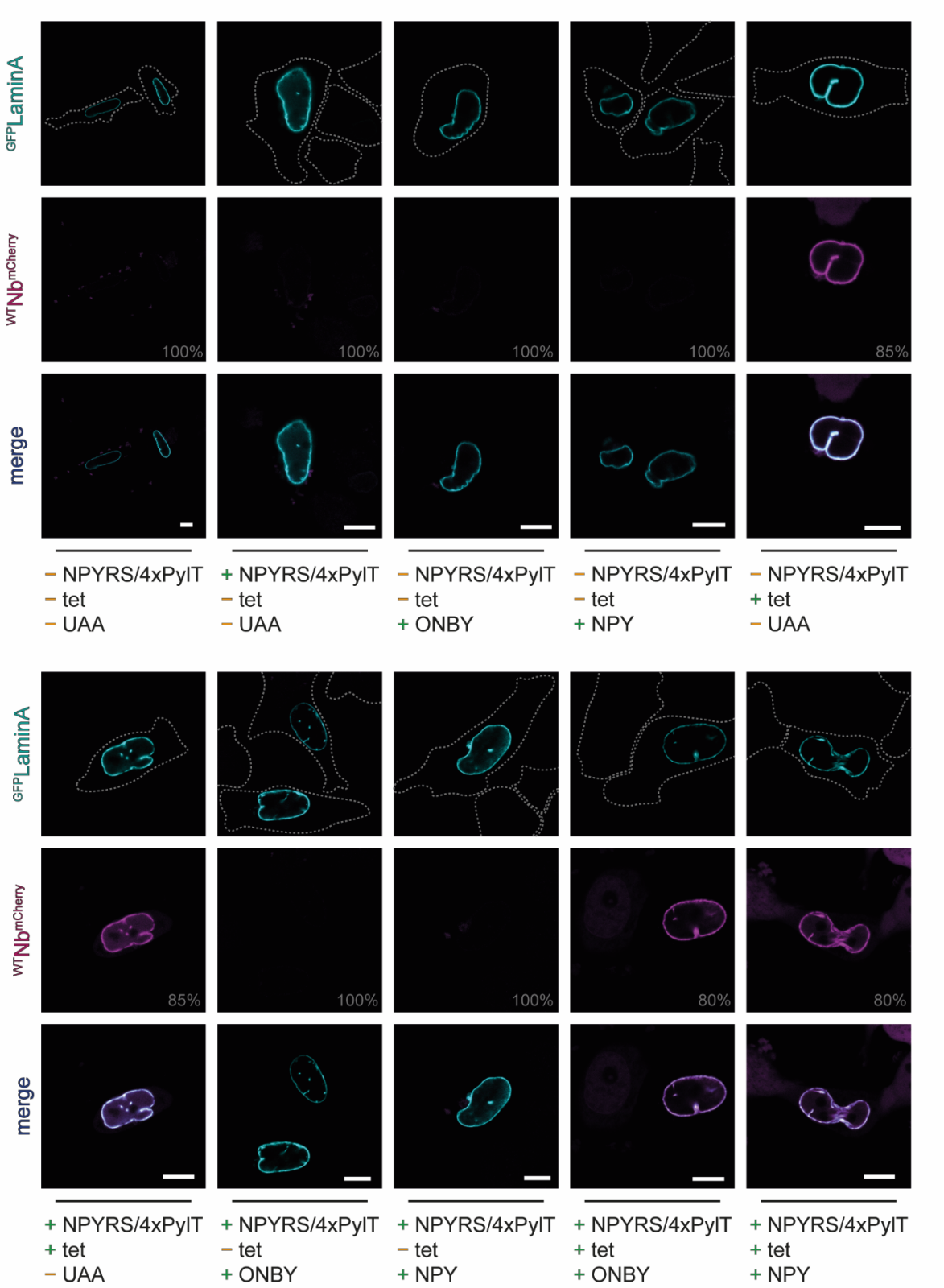

Supplementary Fig. 6 | Constitutively active binding of wild-type intrabody $^{WT}Nb^{mCherry}$ to ^{mEGFP}LaminA. Colocalization visualized by intrabody $^{WT}Nb^{mCherry}$ binding of target located at the nuclear envelope. Tetracycline-induced expression of a constitutively active intrabody resulted in binding. Binding was unaffected by the presence of amber suppression components. CLSM live cell imaging of stable cell line and relative gain indicated in grey. Dashed lines indicate cellular borders. Scale bar, 10 µm.

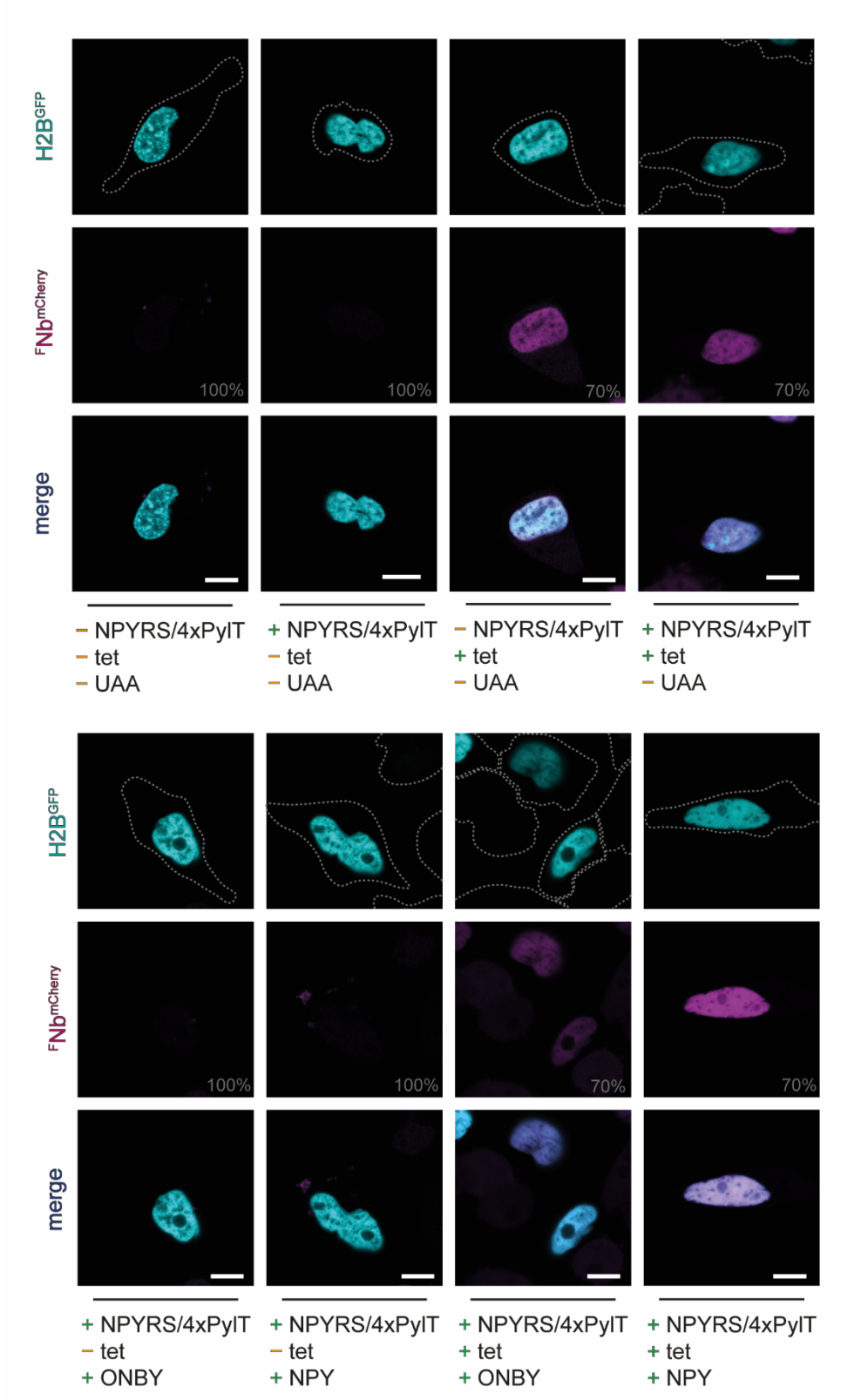

Supplementary Fig. 7 | Constitutively active binding of wild-type $^{WT}Nb^{mCherry}$ to histone $H2B^{EGFP}$. Colocalization visualized by intrabody binding of target located inside the nucleus. Tetracycline-induced expression of a constitutively active intrabody resulted in binding. Binding was unaffected by the presence of amber suppression components. CLSM live cell imaging of stable cell line and relative gain is indicated in grey. Dashed lines indicate cellular borders. Scale bar, 10 µm.

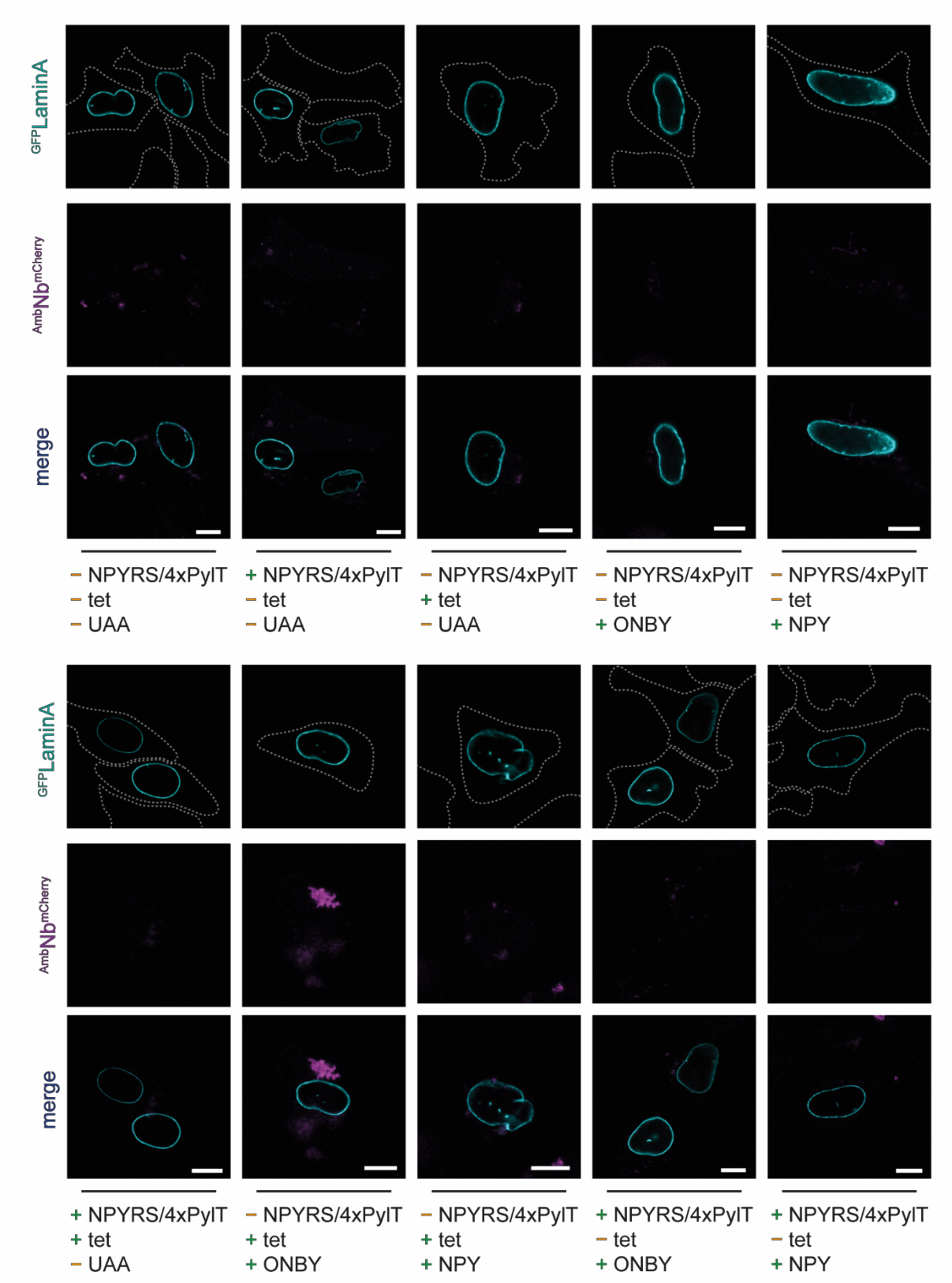

Supplementary Fig. 8 | Abolished translation of $^{Amb}Nb^{mCherry}$ in presence of ^{mEGFP}LaminA. The amber stop codon (Tyr37TAG) abolished expression in the absence of conditions for complete amber suppression. CLSM live cell imaging of stable cell line and relative gain are indicated in grey. Dashed lines indicate cellular borders. Scale bar, 10 µm.

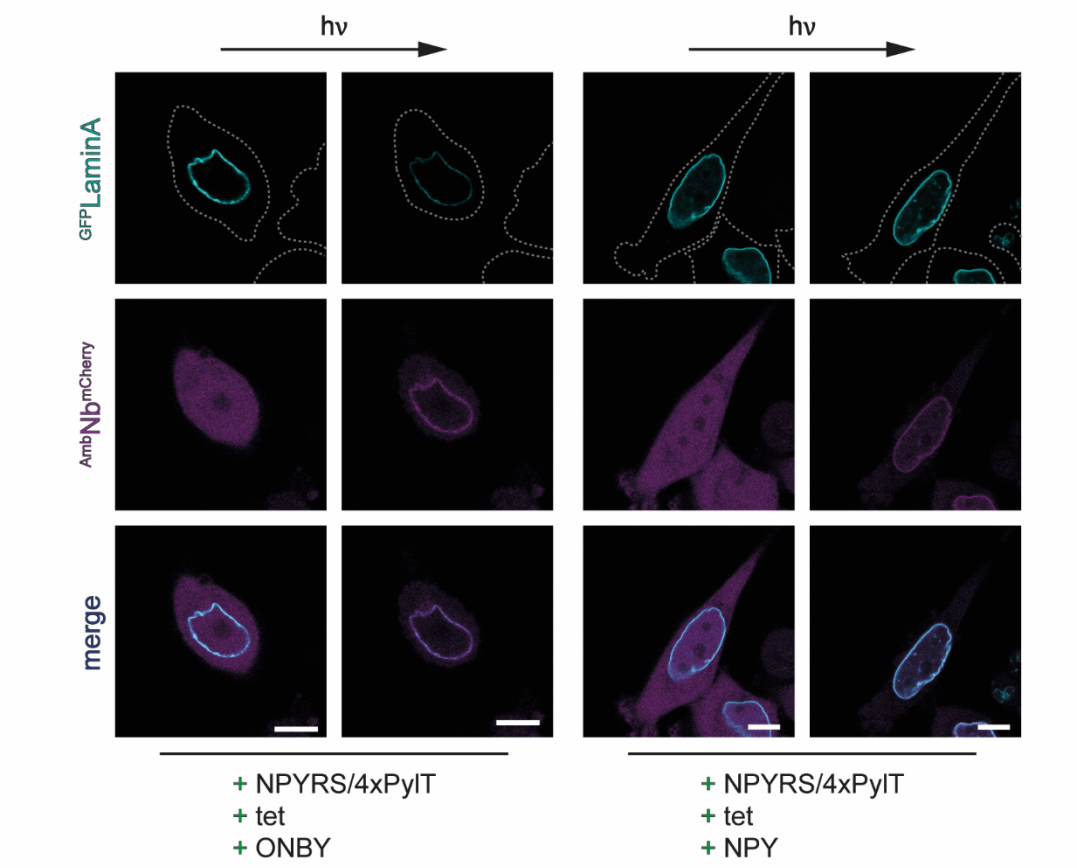

Supplementary Fig. 9 | Photo-activated binding of $^{Amb}Nb^{mCherry}$ to ^{mEGFP}LaminA. Optimized amber-suppression conditions resulted in incorporation of photocaged amino acids. Expression of the amber-suppressed intrabody was monitored by downstream encoded mCherry. The photocaged tyrosines within the epitope-binding site prevented binding. After photo-activation, $^{Amb}Nb^{mCherry}$ binding of target was visualized by colocalization. CLSM live cell imaging of stable cell line. Dashed lines indicate cellular borders. Scale bar, 10 µm. In addition to Supplementary Fig. 7.

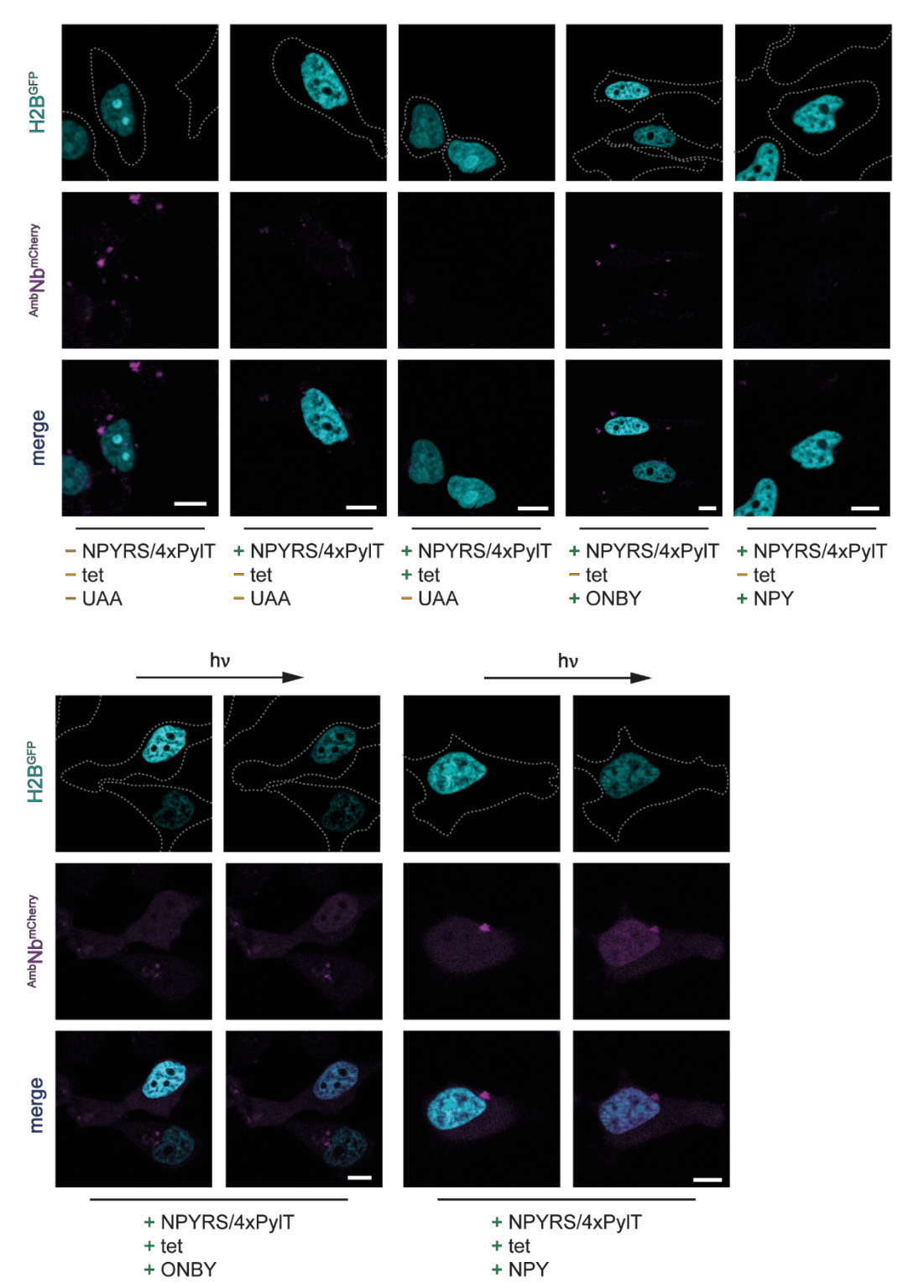

Supplementary Fig. 10 | Photo-induced binding of $^{Amb}Nb^{mCherry}$ to histone $H2B^{EGFP}$. The early amber stop codon (Tyr37*TAG*) abolished expression without complete amber-suppression conditions. Optimized amber-suppression conditions resulted in incorporation of photocaged amino acids. Expression of the amber-suppressed intrabody was monitored by downstream-encoded mCherry. The photocaged tyrosines within the epitope-binding site prevented binding. After photo-activation, instantaneous $^{Amb}Nb^{mCherry}$ binding of target was visualized by colocalisation. CLSM live cell imaging of stable cell line. Dashed lines indicate cellular borders. Scale bar, 10 µm.

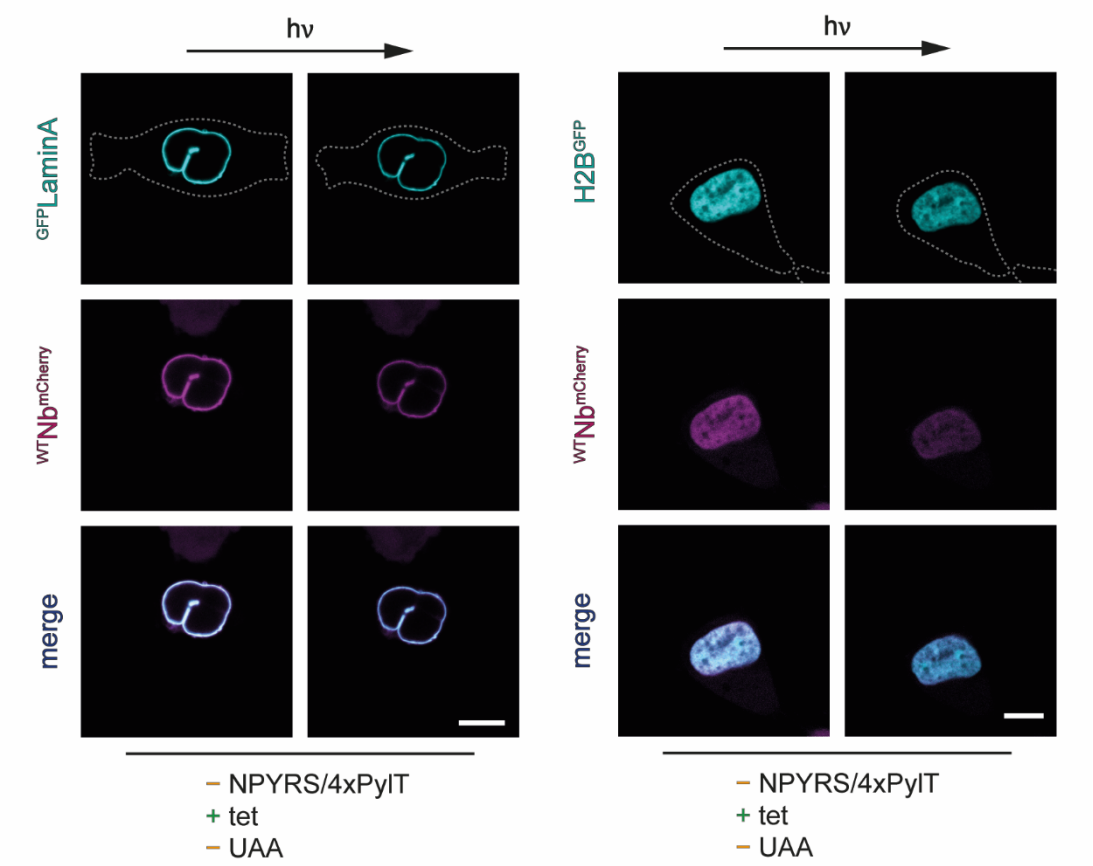

Supplementary Fig. 11 | Constitutively active binding of wild-type intrabody $^{WT}Nb^{mCherry}$ to target proteins is unaffected by light exposure. After tetracycline-induced expression, the constitutively active intrabody showed target binding. Colocalization remained unaffected after light exposure (compared to Supplementary Fig. 8 and 9). Live-cell CLSM imaging of stable cell line. Dashed lines indicate cell border. Scale bar, 10 µm.

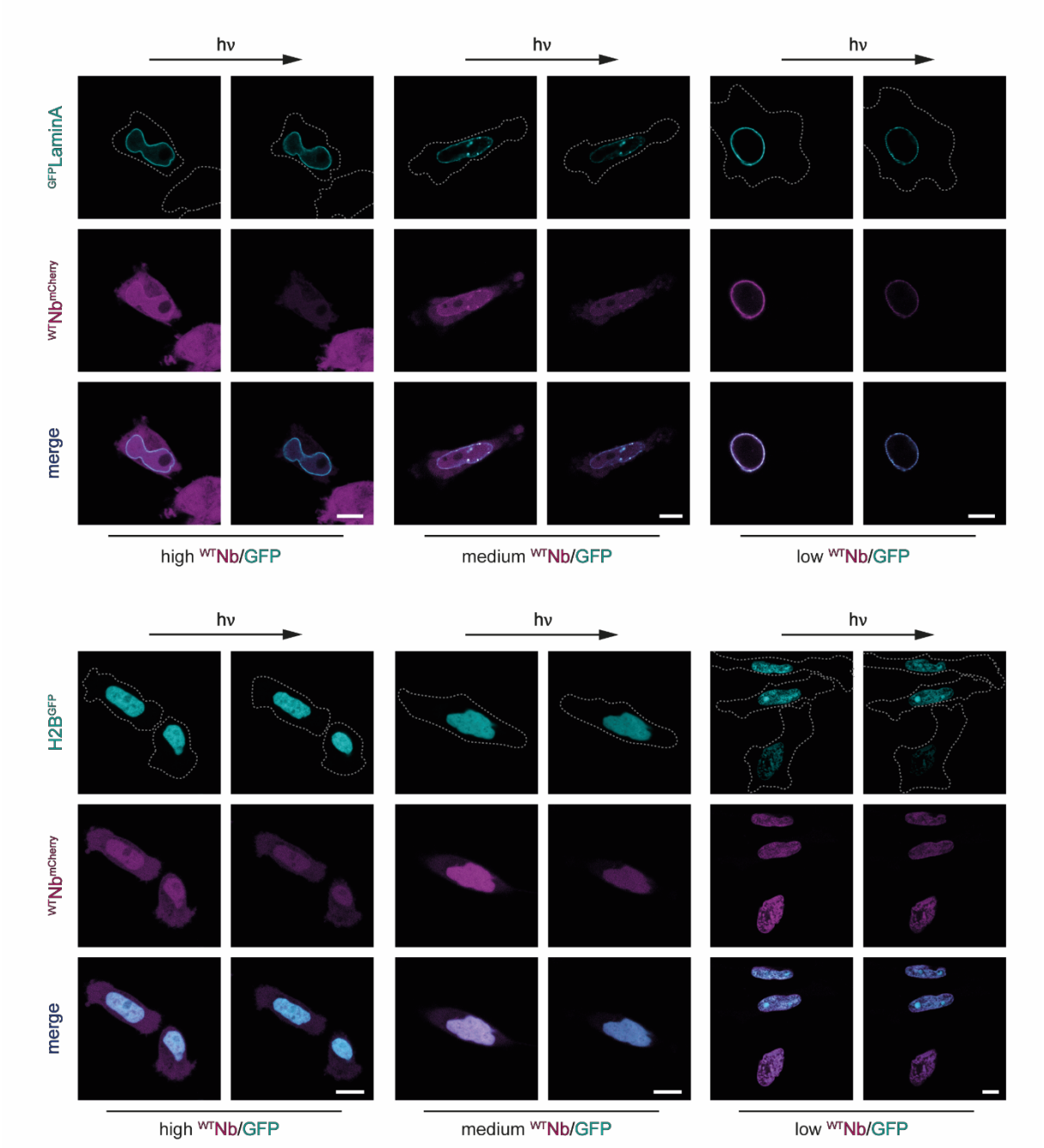

Supplementary Fig. 12 | Unaffected binding of $^{WT}Nb^{mCherry}$ after illumination. After tetracycline-induced expression, the intrabody showed target binding. Colocalization remained unaffected after light exposure (compared to Supplementary Fig. 7 and 8). Live-cell CLSM imaging of stable cell line. Dashed lines indicate cell border. Scale bar, 10 µm.

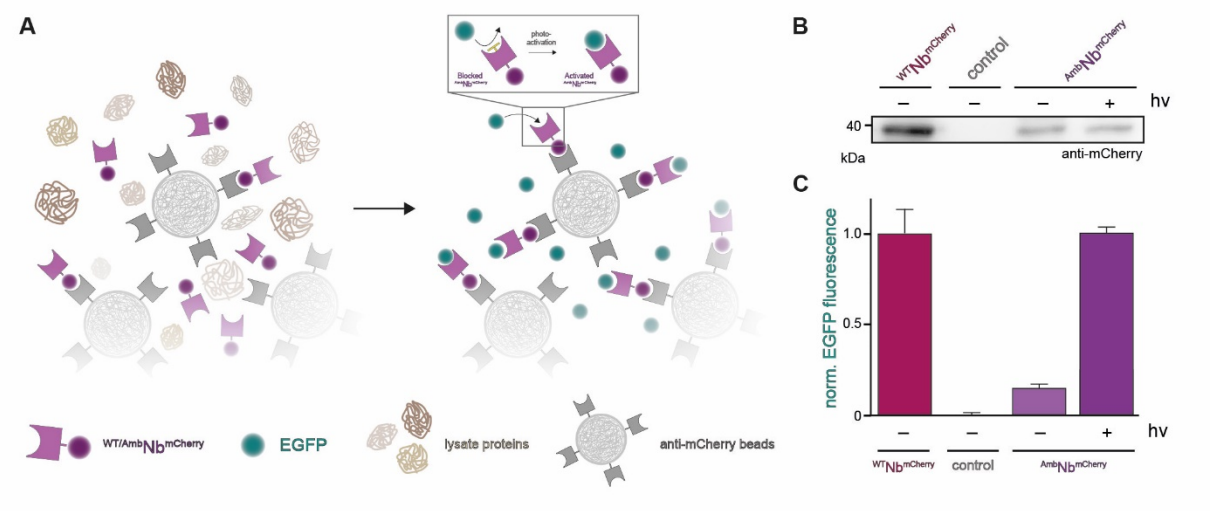

Supplementary Fig. 13 | Photo-activated nanobody binding in human cell lysates. (A) Scheme of the GFP-binding analysis in cell lysates. $^{WT}Nb^{mCherry}$ or $^{Amb}Nb^{mCherry}$ were captured in the cell lysate using anti-mCherry affinity beads. Beads loaded with $^{WT}Nb^{mCherry}$ or $^{Amb}Nb^{mCherry}$ were examined for EGFP binding. After washing, the amount of EGFP coimmunoprecipitated on the beads was quantified by fluorescence. (B) The amount of catpured $^{WT}Nb^{mCherry}$ or $^{Amb}Nb^{mCherry}$ was revealed by immunoblotting. Beads were incubated with 0.5 mg of $^{WT}Nb^{mCherry}$ containing lysate or 1 mg of $^{Amb}Nb^{mCherry}$ containing lysate and 120 nM EGFP. Lysates were pooled from three individual cell preparations. For $^{Amb}Nb^{mCherry}$ amber suppression, ONBY was used. (C) EGFP binding by $^{WT}Nb^{mCherry}$ or $^{Amb}Nb^{mCherry}$. Exposing the cell lysate to UV light restored the epitope binding of $^{Amb}Nb^{mCherry}$. In contrast, only neglectable amounts of EGFP were recorded using beads with unexposed $^{Amb}Nb^{mCherry}$ lysates. EGFP fluorescence was normalized to the amount of captured $^{WT}Nb^{mCherry}$ as illustrated in (B). Means ± SD (n = 3, technical replicates) are displayed.

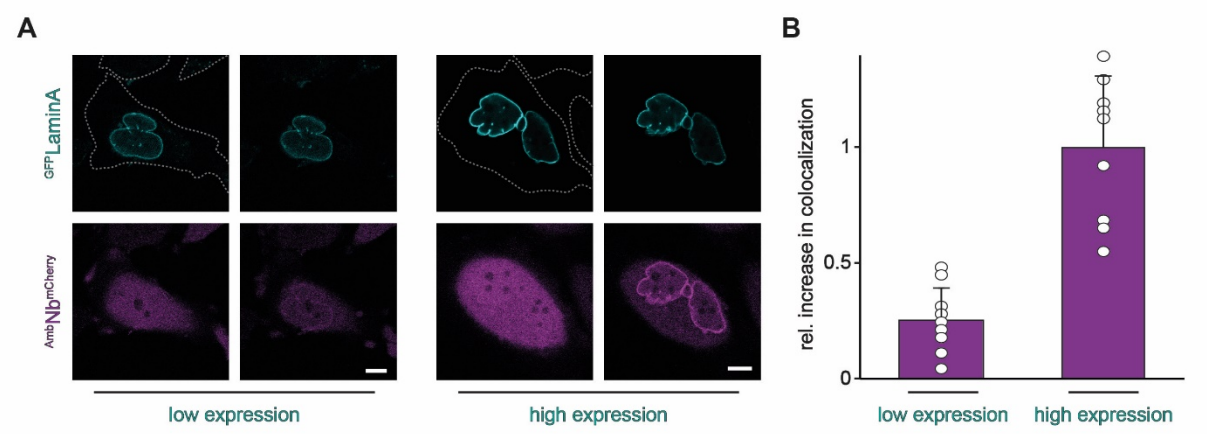

Supplementary Fig. 14 | Statistical analysis of photo-activated intrabody binding. (A) Intrabody binding after illumination inside cells containing low (GFP gain 75%) or high (GFP gain 100%) amounts of target protein. Exemplary cells of two separate groups used in (B). Scale bar, 10 µm. (B) Statistical analysis of photo-activated binding inside two groups of cells with different amount of target protein. Mean increase in colocalization after illumination observed within individual cells (n = 10). For quantification, the absolute increase in colocalization denoted by the Pearson's coefficient was determined and normalized using the high expression group.

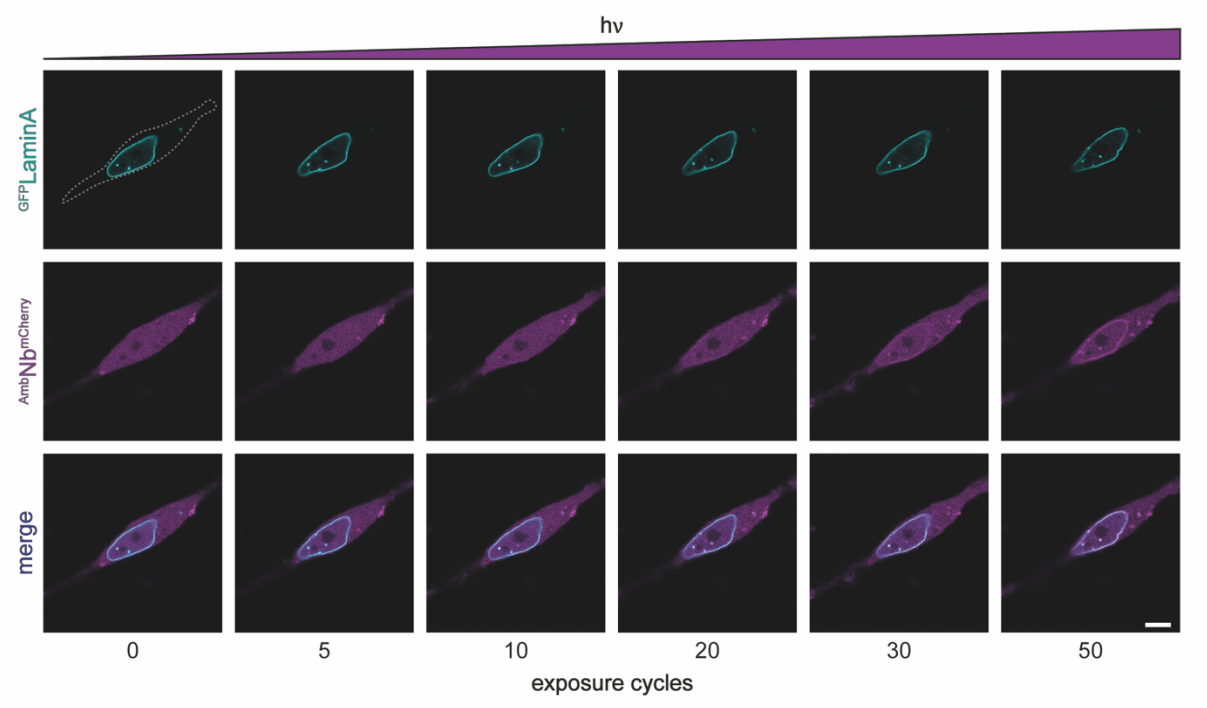

Supplementary Fig. 15 | Dose-dependent ONBY photo-cleavage. After amber suppression using ONBY, no target binding of $^{Amb}Nb^{mCherry}$ was observed. Progressive increase of light exposure allowed tight control of $^{Amb}Nb^{mCherry}$ activation. Intrabody binding was visualized by a correlative increase in target colocalization. Maximum exposure time for photo-activation corresponds to a bleaching function with 250 iterations, 50 cycles, and a 405-nm diode laser (4.5 mW/μm^2) for the whole region of interest. Live-cell CLSM imaging of stable cell line. Dashed lines indicate cell borders. Scale bar, 10 μm.

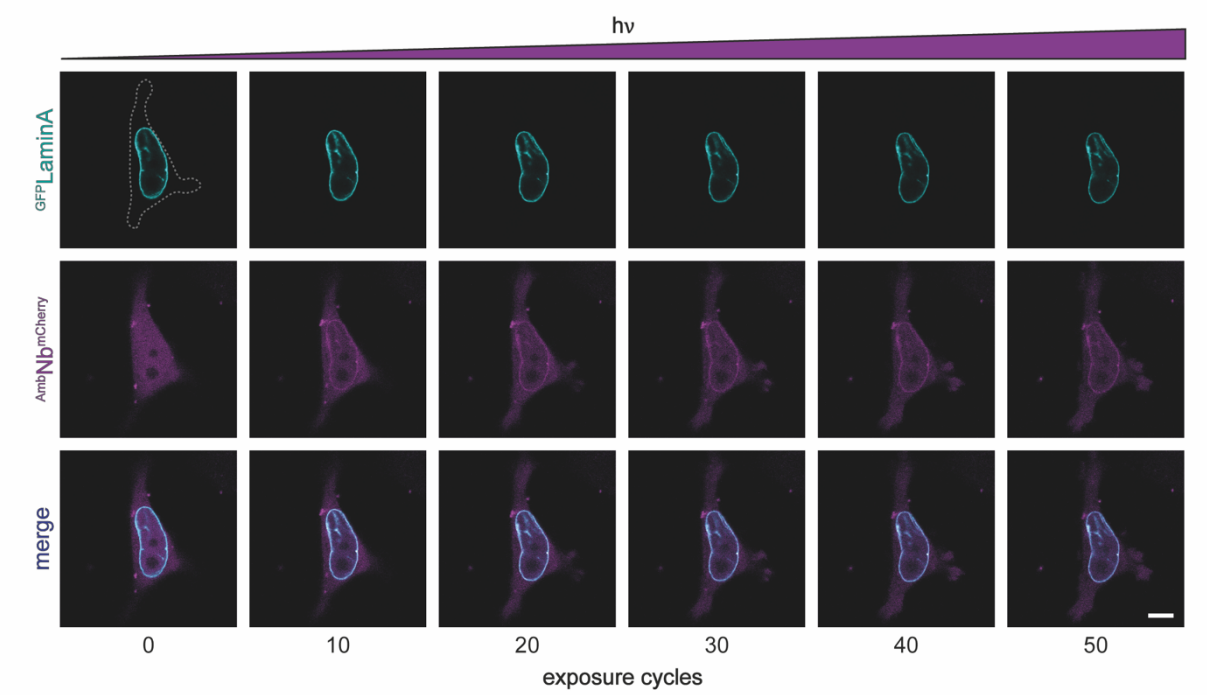

Supplementary Fig. 16 | Dose-dependent NPY photo-cleavage. After amber suppression using NPY, no target preterm binding of $^{Amb}Nb^{mcherry}$ was observed. Progressive increase of light exposure allowed tight control of $^{Amb}Nb^{mCherry}$ activation. Intrabody binding was visualized by a correlative increase in target colocalization. Maximum exposure time for photo-activation corresponds to a bleaching function with 250 iterations, 50 cycles and a 405-nm diode laser (4.5 mW/μm^2) for the whole region of interest. Live-cell CLSM imaging of stable cell line. Dashed lines indicate cell borders. Scale bar, 10 μm.

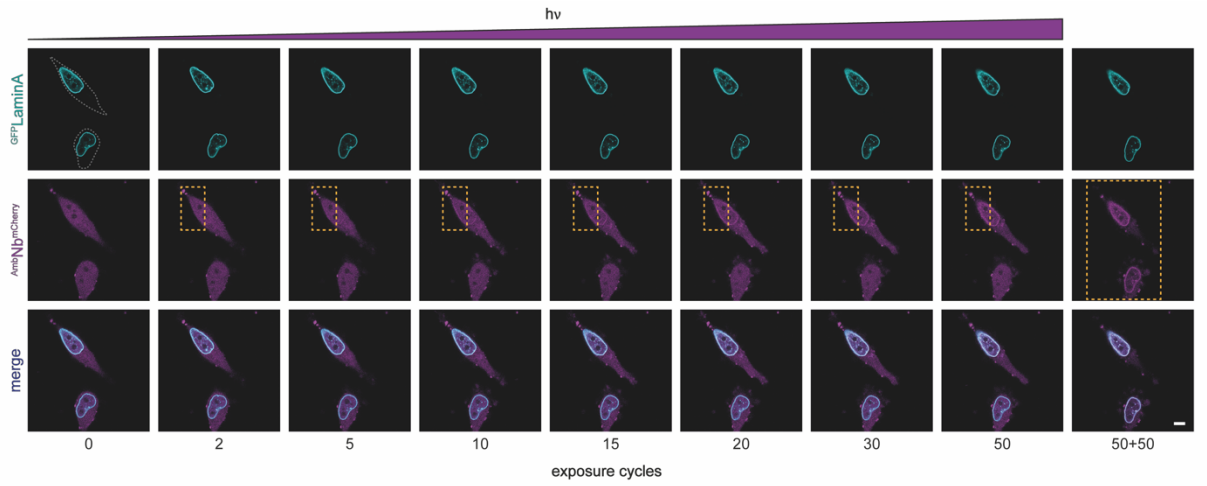

Supplementary Fig. 17 | Fine-tuned intrabody photo-activation by local energy dosage. After amber suppression using NPY, no target-preterm binding of $^{Amb}Nb^{mcherry}$ was observed. A small section of the cell was illuminated with increasing exposure time. Intrabody binding was visualized by a correlative increase in target colocalization. Maximum exposure time for photo-activation corresponds to a bleaching function with 250 iterations, 50 cycles and a 405-nm diode (4.5 mW/μm^2) for the whole region of interest. Live-cell CLSM imaging of stable cell line. Dashed lines indicate cell borders. Scale bar, 10 μm.

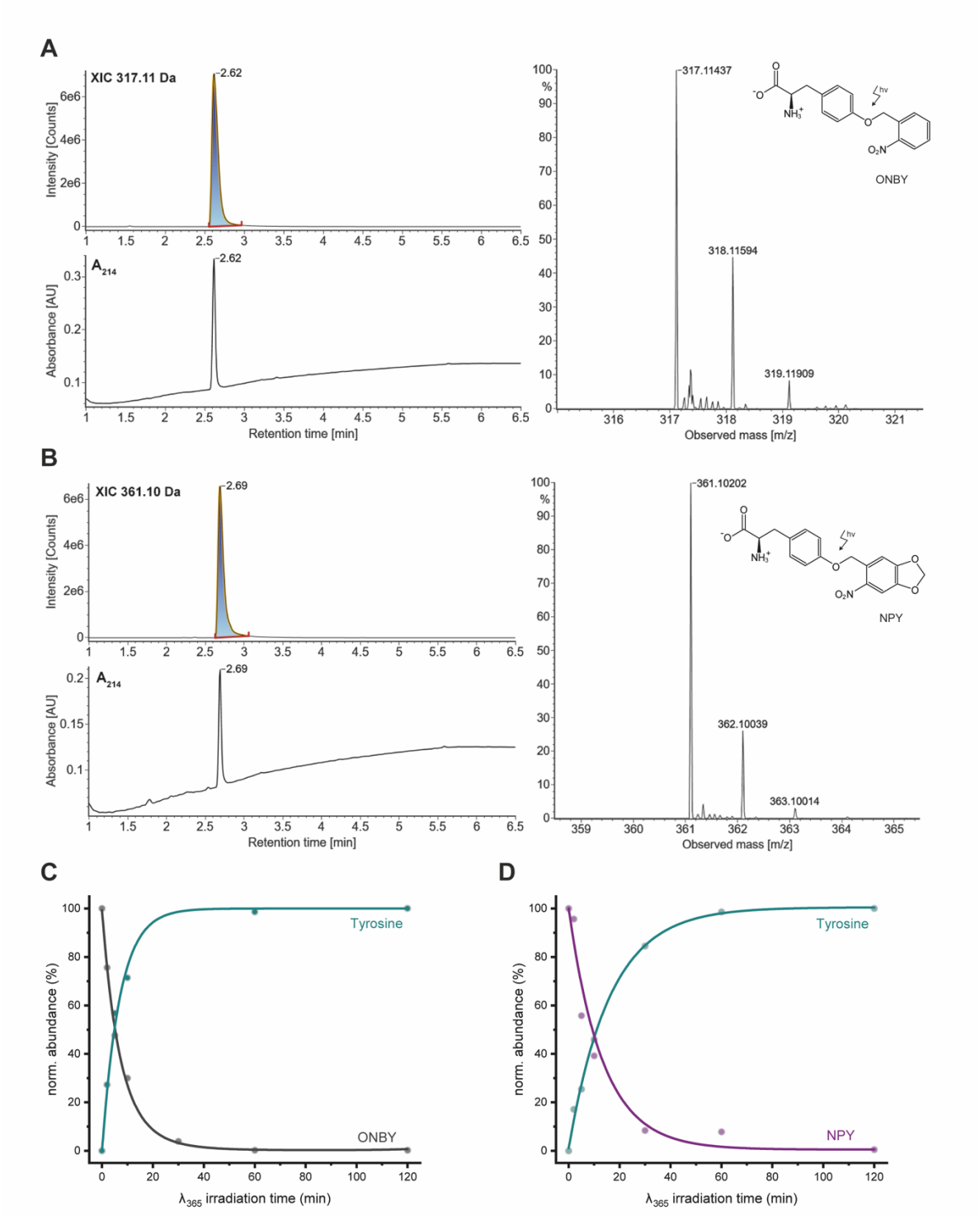

Supplementary Fig. 18 | High-resolution mass analysis of photocaged tyrosines. (A, B) The photocaged tyrosines ONBY (A) or NPY (B) were analyzed by LC-MS. Integrity of (A) ONBY (M_{calc}: 316.1059 Da; M_{obs}: 316.1050 Da [-2.8 ppm]) and (B) NPY (M_{calc}: 360.0958 Da; M_{obs}: 360.0946 Da [-3.2 ppm]) was verified by a cone voltage of 30V, capillary voltage of 0.8 kV in positive polarity. (C, D) Photo cleavage performed in neutral pH PBS using 100 µM of either ONBY (C) or NPY (D). Samples were irradiated with 365 nm (100 mW) for different periods of time. For ONBY and NPY, the peak height at 214 nm was normalized to the uncleaved sample and fitted with a monoexponential decay function. Half-life times were estimated to be 5.0 s for ONBY and 9.1 s for NPY. For uncaged tyrosine, the ESI-MS detector response was used instead.